

Green Synthesis of Iron Oxide Nanoparticles and Their Catalytic and In Vitro Anticancer Activities

P. C. Nagajyothi¹ · Muthuraman Pandurangan² ·
Doo Hwan Kim² · T. V. M. Sreekanth³ ·
Jaesool Shim¹

Received: 10 August 2016 / Published online: 1 October 2016
© Springer Science+Business Media New York 2016

Abstract The green synthesis of nanoparticles is a convenient, inexpensive, rapid and eco-friendly method compared to traditional synthesis methods. We synthesized iron oxide nanoparticles (α -Fe₂O₃ (hematite)) nanoparticles from iron (III) chloride using an aqueous extract of *Psoralea corylifolia* seeds as a reducing agent. Various characterization methods indicate that nanoparticles were crystalline with an average size of ~39 nm. The nanoparticles were assessed for their catalytic activity on methylene blue using a UV–Vis spectrophotometer and showed a rapid reduction within 63 min. The in vitro anticancer activity of the nanoparticles was also determined by Sulforhodamine (SRB) assay, and caspase-3 expression was determined using caspase-3 fluorescence and immunofluorescence assays. The results were suggested the strong cancer cell growth inhibition in a dose-dependent manner.

Keywords Green synthesis · Iron oxide nanoparticles · *Psoralea corylifolia* · Catalytic activity · In-vitro anticancer activity

P.C. Nagajyothi and Muthuraman Pandurangan has contributed equally to this work.

✉ T. V. M. Sreekanth
tvmsreekanth@gmail.com

✉ Jaesool Shim
jshim@ynu.ac.kr

¹ School of Mechanical Engineering, Yeungnam University, 214-1 Dae-dong, Gyeongsan-si, Gyeongsangbuk-do 712-749, Republic of Korea

² Dept of Bioresources and Food Science, Konkuk University, Seoul, South Korea

³ School of Chemical Engineering, Yeungnam University, 214-1 Dae-dong, Gyeongsan-si, Gyeongsangbuk-do 712-749, Republic of Korea

Introduction

Iron oxide nanoparticles are important in catalysis [1], magnetic storage media [2], magnetic inks for jet printing [3], ferrofluids [4], biosensors [5], and wastewater treatment [6]. These nanoparticles are used to their small size, high magnetism, low toxicity, and microwave absorption properties [7]. Nanoparticles have been extensively used in biomedical applications such as anticancer, antimicrobial, mosquitocidal [8–11], larvicidal [12] antiplasmodial [13], ovicidal and larvicidal potential on malaria, dengue and filariasis mosquito Vectors [14, 15]. In addition, green synthesized nanoparticles as inhibitors of dengue growth [16, 17]. Among several nanoparticles, iron oxide nanoparticles with appropriate surface chemistry can be used for various medical applications, such as immunoassay, tissue repair detoxification of biological fluids, cell separation and hyperthermia [18], targeted drug delivery [19], cancer therapy [20], and MRI contrast enhancement [21]. Cancer is one of the major global health problems and involves uncontrolled cell growth with dramatical changes in biochemical and enzymatic parameters [22]. Kidney cancer is the eleventh most common in both men and women and accounts for almost 2 % of all cancers, with an incidence rate of 169,155 and mortality rate of 466,631 per 100, 000 people worldwide [23]. Surgery, chemotherapy, radiation, immunotherapy, and hormones are the primary treatments for cancer, but chemotherapy is predominantly used. However, the chemotherapy not only kills the cancer cells but also affects the normal cells. All of these treatment methods are also expensive, and the can have limited efficacy, toxicity, or chances for multidrug resistance [24, 25]. Nanoparticles are smaller than several hundred nanometers, which is comparable to large biological molecules (enzymes, receptors, and antibodies). With the size that is 100 to 10,000 times smaller than human cells, these nanoparticles can offer unprecedented interactions with biomolecules both on the surface of cells and inside them. Nanoparticle treatment could be revolutionary in cancer diagnosis and therapy [26].

A number of methods are available for the synthesis of iron oxide nanoparticles such as sol–gel reactions [27], sonochemical [28], hydrothermal methods [29], polyol methods [30], microemulsion process [31], flow injection synthesis [32], radiolysis [33], microwave methods [34], aerosol pyrolysis [35], and laser pyrolysis [36]. When synthesized by chemical and physical methods, these nanoparticles lose their reactivity due to aggregation [37], magnetism, and dispersibility upon air exposure [38]. Chemical synthesis methods involve toxic chemicals, the formation of hazardous by-products, and contamination from chemical precursors [39]. Therefore, there is growing interest in developing clean, simple, inexpensive, eco-friendly methods for the synthesis of nanoparticles. Bacteria, fungi, algae, and plant extracts can be used in modern alternatives for the production of metal/metal oxide nanoparticles. Green-synthesized nanoparticles are associated with organic substances from plant extracts that improve particle stability. Compared to microbes, plant-mediated nanoparticles are cheap.

Psoralea corylifolia Linn (Fabaceae family) is an annual herb that is distributed extensively in tropical and subtropical regions. The seeds of *P. corylifolia* are

widely used in traditional Ayurvedic and Chinese medicine for the treatment of a cough, asthma, nephritis, vitiligo, and cavities [40, 41]. We synthesized α -Fe₂O₃ nanoparticles using an aqueous seed extract of *P. corylifolia*. We report the catalytic activity of the nanoparticles towards degradation of MB dye as well as their in vitro cytotoxic activity in renal carcinoma cells (Caki-2 cells) and normal Madin-Darby Canine Kidney Epithelial Cells (MDCK).

Materials and Methods

Materials

Iron (III) chloride (FeCl₃, 99 %), sodium borohydride (NaBH₄) and MB (C₁₆H₁₈ClN₃S·3H₂O) were purchased from Sigma–Aldrich (Seoul, South Korea). Dried Dimethyl sulphoxide (DMSO) and sulforhodamine B (SRB) were purchased from Sigma. Dulbecco's Modified Eagle's Medium (DMEM), fetal bovine serum (FBS), penicillin–streptomycin and trypsin–EDTA were obtained from Welgene (Daegu, South Korea). Rabbit polyclonal caspase 3 antibodies (C1815) were purchased from Santa Cruz Biotechnology (Santa Cruz, California, USA). Donkey Anti-Rabbit IgG H&L (FITC) conjugated secondary antibody (GR200554-2) was purchased from Abcam (330 Cambridge Science Park, Cambridge). All the chemicals were used as received.

Methods

Synthesis of Iron Oxide Nanoparticles

Psoralea corylifolia seeds were purchased from a local market in Gyeongsan, South Korea. *P. corylifolia* seeds were washed with DI water to remove any dust or adhesive materials, dried under laboratory conditions, and made into a fine powder, and stored in an air tight container for further use. 5 g of the seed powder was added to 100 mL of DI water and stirred for 30 min at 60 °C. The iron oxide nanoparticles were synthesized by a previously reported method [42] with slight modification. 10 mL of aqueous seed extract was added to 90 mL of an aqueous solution of 1 mM of Iron (III) chloride solution. The mixture was stirred at 70 °C for 2 h, and the color of the solution changed to dark brown, indicating the formation of the nanoparticles. The nanoparticles were isolated by centrifugation at 15,000 rpm and 4 °C for around 20 min. We repeated this method twice to remove any biomaterials on the surface of the nanoparticles. The nanoparticles were stored in an airtight container in a vacuum desiccator for further use.

Characterization

The nanoparticles were characterized by the different type of instruments like functional groups, and the chemical composition was analyzed by Fourier transform infrared spectroscopy (FT-IR, Perkin-Elmer-Spectrum Two). Raman studies were

done using Raman spectroscopy (Horiba, XploRA series, PLUS). The spectrum was obtained by recording at a wavelength of 400 to 4000 cm^{-1} . X-ray diffraction (XRD) analysis (PANalytical X'Pert MRD) was done using Cu $K\alpha$ radiation ($\lambda = 1.54 \text{ \AA}$) at 40 kV and 30 mA. The shape and morphology of the nanoparticles were determined by scanning electron microscopy (SEM, Hitachi s-4200 N), energy dispersive X-ray analysis (EDAX), and elemental mapping was using the same instrument. High-resolution transmission electron microscopy (HR-TEM-FEI-Tecni TF 20) and selected area diffraction (SAED) were also performed.

Catalytic Experiment

We examined the degradation of the synthetic organic dye MB by NaBH_4 using $\alpha\text{-Fe}_2\text{O}_3$ nanoparticles as a catalyst [43]. MB is used widely as a redox indicator in analytical chemistry. An aqueous solution of this substance is blue in an oxidizing environment and turns colorless when exposed to reducing agents. Its redox properties can be observed in a classical demonstration of chemical kinetics called the “blue bottle” experiment. MB can also be used as a staining dye in many reactions, such as Wright’s stain and Jenner’s stain.

In a typical experiment, 5 mL of NaBH_4 (0.01 M) was mixed with 50 mL of an aqueous solution of MB (1×10^{-3} M) in a beaker, and 25 mg of nanoparticles was then rapidly added with constant stirring. The color of the mixture vanished gradually, indicating the reduction of MB. The catalytic activity of the nanoparticles was evaluated by monitoring the variation in absorbance intensity of the dye solution as a function of time at the corresponding wavelength using a UV–Vis spectrophotometer (OPTIZEN-3220UV).

Cell Culture

MDCK and Caki-2 cells were obtained from ATCC (10801 University Boulevard Manassas, VA 20110 USA). Cells were maintained in growth medium supplemented with 10 % FBS and 1 % antibiotics (penicillin–streptomycin). The cells were grown in a CO_2 incubator at 37 °C and 5 % CO_2 .

SRB Assay

The cytotoxic effect the nanoparticles on the MDCK and Caki-2 cells was measured by SRB assay [44]. Cells were seeded at a density of 2.4×10^4 cells/well into 96-well plates and allowed to adhere for 24 h at 37 °C. Then, the cells were treated for 48 h with nanoparticles at different concentrations (0.01, 0.05, 0.1, 0.2, 0.4 and 0.8 mg/mL). Cells were processed at the end of the treatment, and cytotoxicity was determined.

Caspase-3 Fluorescence Assay

Caki-2 and MDCK cells were cultured (2.4×10^4 cells/well) and treated for 48 h with nanoparticles (0.05, 0.1, 0.2 and 0.4 mg/mL). At the end of treatment, the cells

were centrifuged and the supernatant was removed. Then, 200 μl of caspase-3 assay buffer was added to each tube. 100 μl of cell-based assay lysis buffer was added to the tubes and incubated for 30 min at room temperature. All tubes were centrifuged at $800 \times g$ for 10 min, and 90 μl of the supernatant was transferred to a black 96-well plate. Then, 10 μl of caspase-3 assay buffers and 100 μl of caspase-3 substrate solution were added to each tube. The fluorescence intensity of caspase-3 was measured with excitation at 485 nm and emission at 530 nm (Caspase-3 Fluorescence Assay Kit, Item No-10009135, Cayman Chemical, 1180 East Ellsworth Road Ann Arbor, Michigan 48108 USA).

Immunofluorescence for Caspase-3

Caki-2 cells were cultured (2.4×10^4 cells/well) and treated with nanoparticles (0.2 and 0.4 mg/mL) for 48 h. At the end of treatment, cells were fixed and permeabilized in 0.1 % Triton X-100 in PBS for 20 min and then washed twice with PBS. The blocking was carried out with 3 % bovine serum albumin (BSA) in PBS for 30 min, and the cells were then incubated with Rabbit Polyclonal Caspase-3 antibody for 12 h at 4 °C in PBS-1 % BSA. Cells were washed with PBS and incubated with donkey anti-rabbit IgG H&L (FITC) conjugated secondary antibody. The coverslips were mounted with a fluorescent mounting medium and viewed under a Confocal Laser Scanning Microscope (CLSM) (1×81^R Motorized Inverted Microscope, Olympus) [45].

Statistical Analysis

All the experimental values were expressed mean \pm SD. The difference between control and treated were compared by Student “t” test and followed by ANOVA analysis. A $p < 0.05$ is considered as statistically significant. $^*p < 0.05$. All the treated groups was compared with control ($^*p < 0.05$) and nanoparticles treated groups were compared within the groups ($^ap < 0.05$).

Result and Discussion

Characterization of the Nanoparticles

Figure 1a shows the FT-IR spectra of the nanoparticles. The bands located at 3400 cm^{-1} correspond to O–H stretching (alcohols and phenols), and the bands at 1736 and 1364 cm^{-1} assigned to the C = O stretching (carboxylic acid), and those at 1212 and 1040 cm^{-1} are ascribed to C–N stretching (aliphatic amines). The peaks at 526 and 450 cm^{-1} show the presence of Fe–O bond vibrations from the Fe_2O_3 [46].

Raman spectroscopy was used to learn more about the chemical identity of the nanoparticles, as shown in Fig. 1b. The main features of the wave numbers are located at 222 (A_{1g}), 288 (E_g), 399 (E_g), 492 (A_{1g}), and 605 (E_g) cm^{-1} and there is a broad peak at 1300 cm^{-1} . These results match very well with the Raman modes of

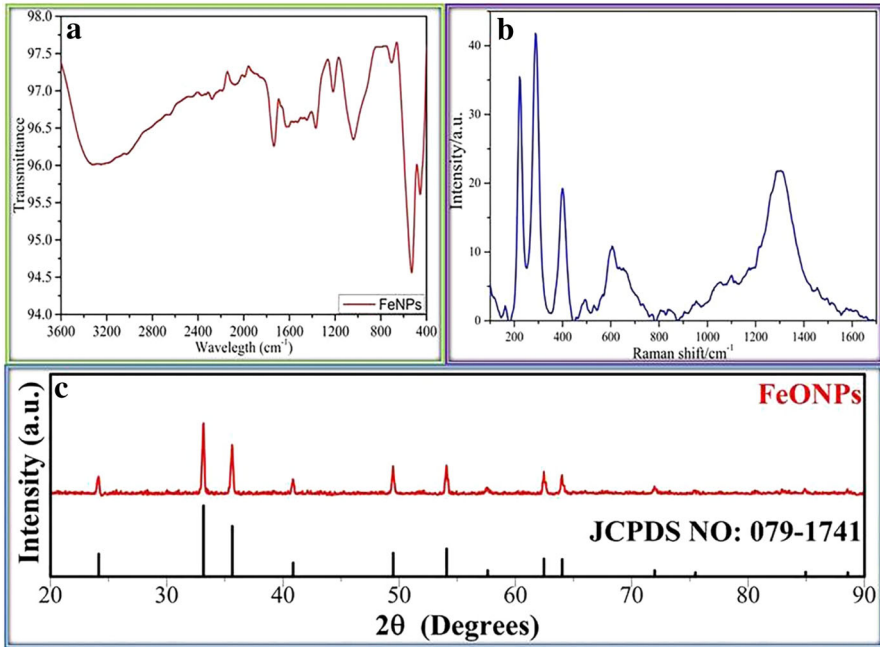


Fig. 1 **a** FT-IR spectrum of greens synthesized α -Fe₂O₃ nanoparticles, **b** Raman spectrum of *green* synthesized α -Fe₂O₃ nanoparticles and **c** XRD pattern of *green*-synthesized α -Fe₂O₃ nanoparticles (Color figure online)

the α -Fe₂O₃ phase [47]. The peaks above 1100 cm⁻¹ are not meant for iron oxide phase identification [19].

The crystalline nature and average size of the nanoparticles were analyzed by XRD as shown in Fig. 1c. The XRD spectrum shows different diffraction peaks at 24.16, 33.24, 35.73, 40.99, 49.49, 54.03, 57.50, 62.53, 64.13, 71.90, 75.57, 85.07 and 88.55°, which correspond to the (012), (104), (110), (113), (024), (116), (018), (214), (300), (1010), (220), (134) and (226) Bragg reflections. These results indicate a rhombohedral α -Fe₂O₃ phase and match with JCPDS card no. 079-1741. The average size of nanoparticles was estimated to be 39 nm according to the Scherrer equation.

The morphologies and size of the nanoparticles were investigated by SEM and HR-TEM. As seen in the SEM images (Fig. 2a–c), the nanoparticles have spherical, rod-like and uneven shapes. The EDAX spectrum and elemental mapping confirms that the as-prepared nanoparticles contain Fe and O as the main elements (Fig. 2d). HR-TEM images show that the nanoparticles were spherical, hexagonal and cubic in shape (Fig. 3a–e). The SAED pattern (Fig. 3f) reveals that the particles are crystalline in nature.

Catalytic Activity of Iron Oxide Nanoparticles

Eco-friendly degradation of MB was performed by NaBH₄ in the presence of the nanoparticles. The characteristic absorption of MB at λ_{max} = 664nm was used to

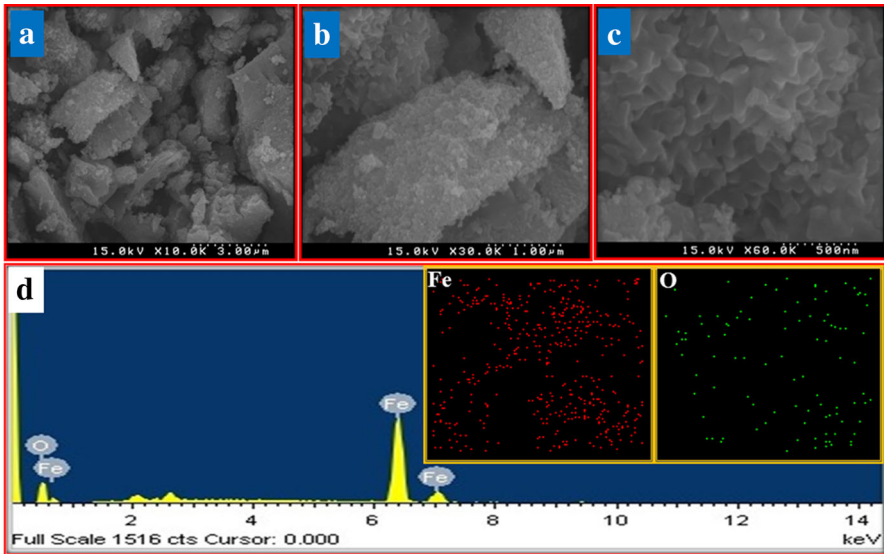


Fig. 2 a–c Scanning electron microscopic images of *green* synthesized α -Fe₂O₃ nanoparticles with different magnification and **d** EDAX spectrum of *green*-synthesized α -Fe₂O₃ nanoparticles; *inset* elemental mapping of iron and oxygen (Color figure online)

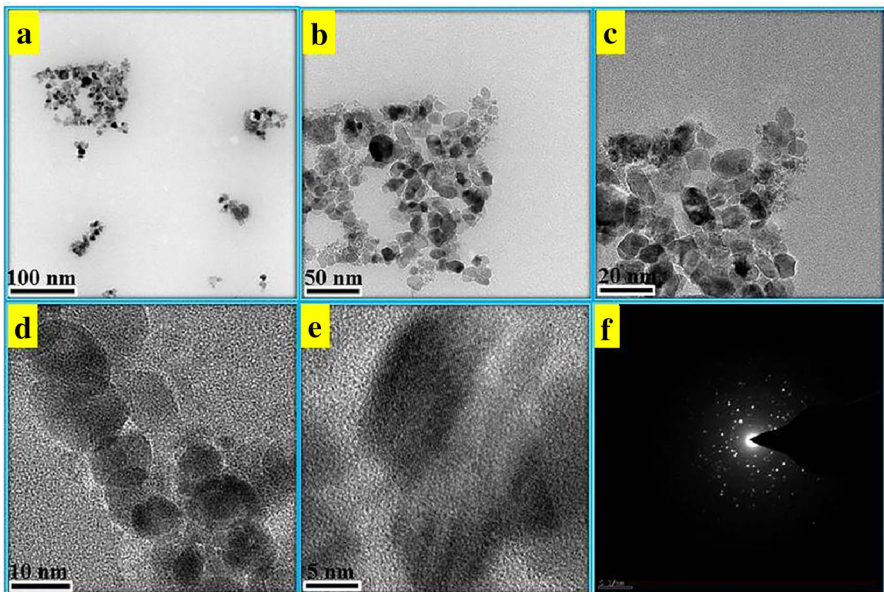


Fig. 3 a–e High resolution electron transmission microscope images at different magnifications and **d** SAED pattern of *green*-synthesized α -Fe₂O₃ nanoparticles

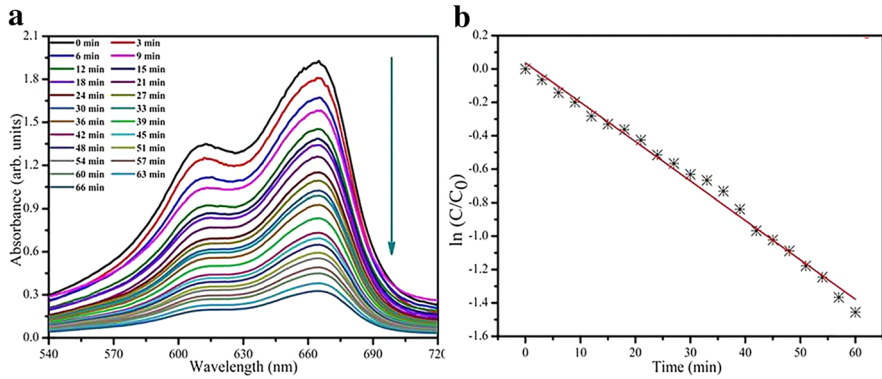


Fig. 4 **a** Time-dependent UV–visible absorption spectra of MB by NaBH₄ in the presence of green-synthesized α -Fe₂O₃ nanoparticles and **b** plot of $\ln(C/C_0)$ as a function of time (Color figure online)

monitor the reaction. The catalytic degradation of MB by NaBH₄ was examined while keeping all other parameters constant. Without the metal catalyst, the mixture of MB and NaBH₄ did not show any appreciable degradation (data not shown). Figure 4a shows the time-dependent variation of absorption spectra for MB degradation by NaBH₄ in the presence of the nanoparticles for up to 63 min. After 60 min, 71.5 % of the initial concentration of MB was degraded. The rate of degradation (d) was calculated by the following equation [48].

$$d = \left(1 - \frac{C}{C_0}\right) \times 100$$

where C and C_0 are the initial and final concentrations of MB dye, and d is the relative degradation percentage of MB (%). According to the Langmuir–Hinshelwood model, the pseudo-first order kinetic equation for a low dye concentration is [49]:

$$\ln\left(\frac{C}{C_0}\right) = -kt$$

where k is the apparent first-order rate constant (min^{-1}), Fig. 4b shows a plot of the pseudo-first order kinetics with respect to time. The slope of the linear fit represents the rate constant (k) for the degradation of the MB dye.

Anticancer Activity of Iron Oxide Nanoparticles

The effect of nanoparticles on cell viability was determined, and the percentage of cell growth inhibition was calculated. A clear concentration-dependent cell growth inhibition was observed with nanoparticle exposure (Fig. 5). Murugan et al. [50] recently reported, TiO₂ NPs exhibited dose dependent cytotoxicity against human breast cancer cells (MCF-7) and normal breast epithelial cells (HBL-100). However, a nanoparticle concentration of 0.8 mg/mL could inhibit the growth of Caki-2 cells,

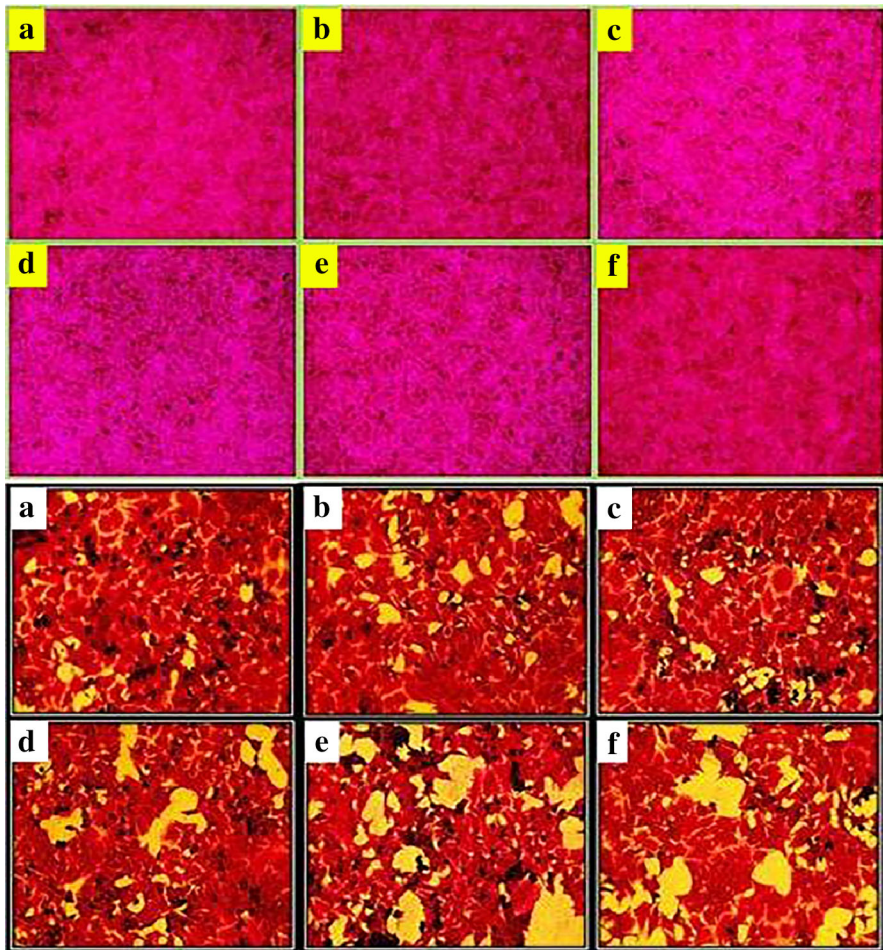


Fig. 5 Cytotoxic effect of α -Fe₂O₃ nanoparticles on MDCK and Caki-2 cells by SRB assay at 48 h. Morphological observation by inverted microscope (40x). Representative images from three independent experiments (Upper is MDCK cells and down is Caki-2 cells; a control, b 0.01 mg/mL, c 0.05 mg/mL, d 0.1 mg/mL, e 0.2 mg/mL, f 0.4 mg/mL)

which suggests that this concentration could be toxic to normal cells. Therefore, this concentration was not used for further study (Fig. 6a). Caspase activity was monitored in the MDCK and Caki-2 cells following exposure to 0.05–0.4 mg/mL of nanoparticles at 48 h. The caspase-3 fluorescence was measured using caspase-3 substrate N-Ac-DEVD-N-MC-R110. The fluorescence significantly increased in MDCK cells at a higher concentration of nanoparticle exposure. The fluorescence gradually increased in the renal carcinoma cells in a concentration-dependent manner (Fig. 6b). These results indicate the occurrence of apoptosis.

Caspase-3 expression was monitored in the Caki-2 cells following exposure to 0.2 and 0.4 mg/mL of at 48 h. The caspase-3 expressions correspond to the

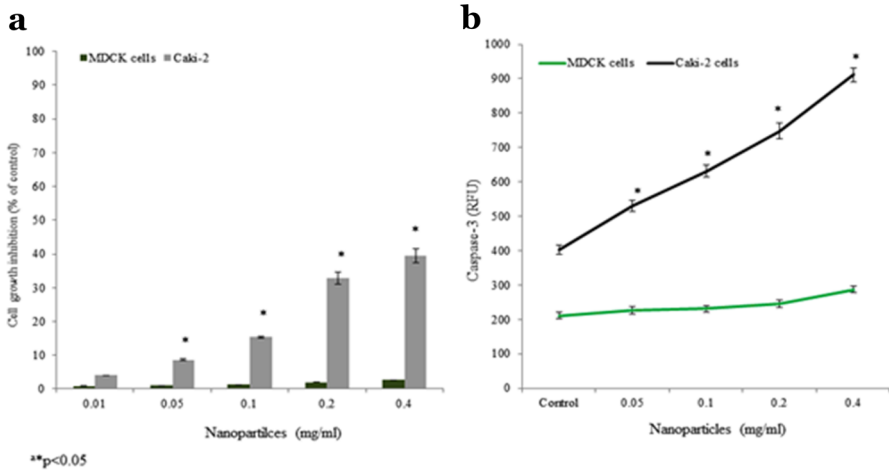


Fig. 6 **a** Cytotoxic effect of α -Fe₂O₃ nanoparticles on MDCK and Caki-2 cells by SRB assay at 48 h. Results were presented as percentage of growth inhibition compared with the control. **b** Effect of α -Fe₂O₃ nanoparticles on caspase 3 fluorescence. Relative fluorescence for caspase- 3 in MDCK and Caki-2 cells following incubation with α -Fe₂O₃ nanoparticles. **p < 0.05

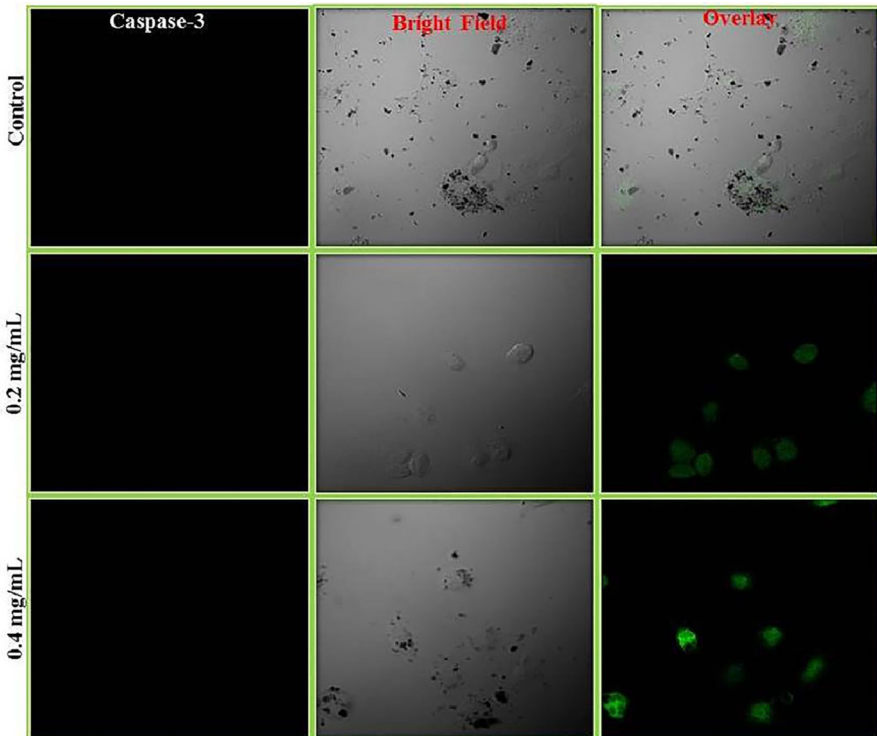


Fig. 7 Effect of α -Fe₂O₃ nanoparticles on caspase-3 expression. Immunofluorescence for caspase-3 in Caki-2 cells following incubation with α -Fe₂O₃ nanoparticles (0.2 and 0.4 mg/mL)

appearance of immunofluorescence in the cytoplasm using caspase-3 antibody. The expressions gradually increased in the renal carcinoma cells in a concentration-dependent manner (Fig. 7). The results confirm the occurrence apoptosis. This result agreed with our previous report about BaCO₃, TiO₂ and AgNPs induced caspase-3 expression in cervical tumor cells [51–53]. Recently, diverse uses for iron oxide nanoparticles have been reported for cancer therapy [54]. Vignesh et al. [55] reported the formulation α -Fe₂O₃ nanoparticles using exopolysaccharide and evaluated their antibacterial and anticancer activities. In-vitro anticancer activity of doxorubicin-loaded gelatin-coated magnetic iron oxide nanoparticles has been reported for cervical tumor cells [56]. Gaihre et al. [57] reported the bioactivity of gelatin coated magnetic iron oxide nanoparticles. Our results agreed with these findings.

Conclusion

Green routes for nanoparticle synthesis are of great interest because they are eco-friendly, inexpensive, simple and rapid. They also have a wide range of applications, such as in nanomedicine, catalysis, and optoelectronics. We showed that α -Fe₂O₃ nanoparticles can be synthesized by a green synthesis method using *P. corylifolia* seeds. The nanoparticles showed efficient catalytic activity towards the degradation of MB dye and could be used in industrial waste water treatment. The size of the nanoparticles was 39 nm according to XRD data, and they revealed a significant anticancer activity against renal tumor cells at lower concentrations.

Acknowledgments This work was supported by the Basic Science Research Program through the National Research Foundation of Korea (NRF) funded by the Ministry of Education (2015R1A2A2A01003741). This work was also supported by KU-Research Professor Program, Konkuk University, Seoul, South Korea.

References

1. J. L. Zhang, Y. Wang, H. Ji, Y. G. Wei, N. Z. Wu, B. J. Zuo, and Q. L. Wang (2005). *J. Catal.* **229**, 114.
2. S. H. Sun, C. B. Murray, D. Weller, L. Folks, and A. Moser (2000). *Science* **287**, 1989.
3. S. W. Charles and J. Popplewell (1982). *Endeavour* **6**, 153.
4. B. Jeyadevan, C. N. Chinnasamy, K. Shinoda, K. Tohji, and H. Oka (2003). *J. Appl. Phys.* **93**, 8450.
5. M. M. Miller, G. A. Prinz, S. F. Cheng, and S. Bounnak (2002). *Appl. Phys. Lett.* **81**, 2211.
6. X. Piao, M. Z. Guang, L. H. Dan, L. F. Chong, H. Shuang, H. Z. Mei, L. Cui, W. Zhen, H. Chao, X. X. Geng, and F. L. Zhi (2012). *Sci. Total Environ.* **424**, 1.
7. R. P. Chang, J. Yu, X. Ma, and D. P. Anderson (2011). *Carbohydr. Polym.* **83**, 640.
8. D. Dinesh, K. Murugan, P. Madhiyazhagan, C. Panneerselvam, M. Nicoletti, W. Jiang, G. Benelli, B. Chandramohan, and U. Suresh (2015). *Parasitol Res* **114**, 1519.
9. A. Jaganathan, K. Murugan, K. Murugan, C. Panneerselvam, P. Madhiyazhagan, D. Dinesh, C. Vadivalagan, A. T. Aziz, B. Chandramohan, U. Suresh, R. Rajaganesh, J. Subramaniam, M. Nicoletti, A. Higuchi, A. Abdullah, A. M. Munusamy, S. Kumar, and G. Benelli (2016). *Parasitol Int* **65**, 276.
10. G. Benelli, A. Lo Iacono, A. Canale, and H. Mehlhorn (2016). *Parasitol Res* **115**, 2131.
11. G. Benelli (2016). *Parasitol Res.* **115**, 23.

12. S. Vincent, K. Kovendan, B. Chandramohan, K. Siva, P. Mahesh Kumar, C. Vasugi, C. Praseeja, J. Subramaniam, M. Govindarajan, K. Murugan, and G. Benelli (2016). *J. Clust. Sci.* doi:[10.1007/s10876-016-1038-3](https://doi.org/10.1007/s10876-016-1038-3).
13. M. Govindarajan and G. Benelli (2016). *J. Clust. Sci.* doi:[10.1007/s10876-016-1035-6](https://doi.org/10.1007/s10876-016-1035-6).
14. M. Govindarajan, M. Nicoletti, and G. Benelli (2016). *J. Clust. Sci.* **27**, 745.
15. K. Murugan, N. Aarthi, K. Kovendan, C. Panneerselvam, B. Chandramohan, P. Mahesh Kumar, D. Amerasan, M. Paulpandi, R. Chandirasekar, D. Dinesh, U. Suresh, J. Subramaniam, A. Higuchi, A. A. Alarfaj, M. Nicoletti, H. Mehlhorn, and G. Benelli (2015). *Parasitol Res* **114**, 4087.
16. G. Benelli (2016). *Asia Pacif J. Trop. Biomed.* doi:[10.1016/j.apjtb.2015.10.015](https://doi.org/10.1016/j.apjtb.2015.10.015).
17. G. Benelli and H. Mehlhorn (2016). *Parasitol Res.* **115**, 1747.
18. A. K. Gupta and M. Gupta (2005). *Biomaterials* **26**, 3995.
19. I. Chourpa, L. Douziech-Eyrolles, L. Ngaboni-Okassa, J. F. Fouquenot, S. Cohen-Jonathan, M. Souce, H. Marchais, and P. Dubois (2005). *Analyst* **130**, 1395.
20. H. Pardoe, P. R. Clark, T. G. St Pierre, P. Moroz, and S. K. A. Jones (2003). *Magn. Reson. Imag* **21**, 483.
21. C. Burtea, S. Laurent, A. Roch, L. Vander Elst, and R. N. Muller (2005). *Inorg. Biochem.* **99**, 1135.
22. K. Palaniselvam, M. M. Yusoff, G. P. Maniam, and G. Natanamurugaraj (2015). *Saudi Pharma. J.* doi:[10.1016/j.jsps.2014.11.013](https://doi.org/10.1016/j.jsps.2014.11.013).
23. Kidney cancer incidence and mortality worldwide in 2008: Globocan Cancer Fact Sheet, *Globocan 2008*, IARC, 2010.
24. R. V. Ancuceanu and V. Istudor (2004). *Alter. Med. Rev.* **9**, 402.
25. W. Tan, J. Lu, M. Huang, Y. Li, M. Chen, G. Wu, J. Gong, Z. Zhong, Z. Xu, Y. Dang, J. Guo, X. Chen, and Y. Wang (2011). *Chine. Med.* **6**, 15.
26. R. Seigneuric, L. Markey, D. S. A. Nuyten, C. Dubernet, C. T. A. Evelo, E. Finot, and C. Garrido (2010). *Curr. Mol. Med.* **10**, 640.
27. B. Samira, K. G. Chandrappa, and S. B. Abd Hamid (2013). *Res. J. Chem. Sci* **3**, 62.
28. R. Vijayakumar, Yu Koltypin, I. Felner, and A. Gedanken (2000). *Mat. Sci. Eng. A* **286**, 101.
29. S. Giri, S. Samanta, S. Maji, S. Ganguli, and A. Bhaumik (2005). *J. Magn. Magn. Mater.* **285**, 296.
30. W. Cai and J. J. Wan (2007). *Collo. Inter. Sci.* **305**, 366.
31. J. Vidal-Vidal, J. Rivas, and M. A. López-Quintela (2006). *Collo. Surf. A* **288**, 44.
32. G. S. Alvarez, M. Muhammed, and A. A. Zagorodni (2006). *Chem. Eng. Sci.* **61**, 4625.
33. A. Alam, D. Abdul Razak, M. A. Abdul Hamid, and N. Kamil Othman (2014). *Plos One* **9**, e90055.
34. C. Elisa, B. Verónica, M. Anna, M. Joan, R. Anna, and R. Anna (2014). *Acta. Biomat.* **10**, 3775.
35. P. Tartaj, T. Gonzalez-Carreno, and C. J. Serna (2004). *Adv. Mater.* **16**, 529.
36. O. Bomati-Miguel, L. Mazeina, A. Navrotsky, and S. Veintemillas Verdaguera (2008). *Chem. Mater.* **20**, 591.
37. J. H. Kim, P. G. Tratnyek, and Y. S. Chang (2008). *Environ. Sci. Technol.* **42**, 4106.
38. W. Wu, Q. He, and C. Jiang (2008). *Nanoscale Res. Lett.* **3**, 397.
39. K. N. Thakkar, S. S. Mhatre, and R. Y. Parikh (2010). *Nanomed.* **6**, 257–262.
40. J. Y. Peng, G. R. Fan, and Y. T. Wu (2006). *J Chromato A* **1115**, 103–111.
41. R. M. Liu, A. F. Li, A. L. Sun, and L. Y. Kong (2004). *J. Chromato. A* **1057**, 225.
42. M. Kanchan, B. Nagaraj, and Y. R. Lee (2015). *Cataly. Sci. Technol.* **5**, 2612.
43. T. V. M. Sreekanth, G. R. Dillip, and Y. R. Lee (2016). *Cera. Int.* **42**, 6610.
44. P. Muthuraman, E. Gansukh, M. Bhupendra, C. Murugesan, N. Rafi, and K. D. Hwan (2015). *Saudi J. Biol. Sci.* doi:[10.1016/j.sjbs.2015.06.01](https://doi.org/10.1016/j.sjbs.2015.06.01).
45. P. Muthuraman (2014). *Appli. Biochem. Biotechnol.* **173**, 980.
46. K. Brajesh, K. Smita, C. Luis, and D. Alexis (2014). *J. Saudi Chem. Soc.* **18**, 364.
47. C. Young-Sik and H. Young-Duk (2009). *Bull. Korean. Chem. Soc.* **30**, 1413.
48. G. R. Dillip, A. N. Banerjee, V. C. Anitha, S. W. Joo, B. K. Min, S. Y. Sawant, and M. H. Cho (2015). *Chem. Phys. Chem.* **16**, 3214.
49. T. D. Dang, A. N. Banerjee, S. W. Joo, and B. K. Min (2014). *Ind. Eng. Chem. Res.* **53**, 9743.
50. K. Murugan, D. Dinesh, K. Kavithaa, M. Paulpandi, T. Ponraj, M. Saleh Alsalhi, S. Devanesan, J. Subramaniam, R. Rajaganesh, H. Wei, K. Suresh, M. Nicoletti, and G. Benelli (2016). *Parasitol Res* **115**, 1085.
51. P. C. Nagajyothi, P. Muthuraman, T. V. M. Sreekanth, and J. Shim (2016). *J. Photochem. Photobiol. B* **156**, 29.
52. P. Muthuraman, G. Enkhtaivan, B. Venkitasamy, B. Mistry, R. Noorzai, B. Y. Jin, and D. H. Kim (2016). *Biol. Trace. Elem. Res.* **170**, 309.

53. P. Muthuraman, E. Gansukh, J. A. Young, and D. H. Kim (2015). *Biol. Trace Elem. Res.* doi:[10.1007/s12011-015-0551-9](https://doi.org/10.1007/s12011-015-0551-9).
54. G. S. Abayaweera (2014). Diverse use of iron oxide nanoparticles for anticancer therapy. Kansas State University. Ph.D. Thesis. 2014.
55. V. Vignesh, G. Sathiyarayanan, G. Sathishkumar, K. Parthiban, K. Sathishkumar, and R. Thirumurugan (2015). *RSC Adv.* **5**, 27794.
56. B. Gaihre, M. S. Khil, and H. Y. Kim (2011). *J. Microencapsul.* **28**, 286.
57. B. Gaihre, M. S. Khil, H. K. Kang, and H. Y. Kim (2009). *J. Mat. Sci. Mat. Med.* **20**, 573.